World Scientific
www.worldscientific.com

Non-Markovianity by undersampling in quantum optical simulators

Matteo A. C. Rossi*, Claudia Benedetti and Dario Tamascelli

Quantum Technology Lab, Dipartimento di Fisica
Università di Milano, I-20133 Milano, Italy
*matteo.rossi@fisica.unimi.it

Simone Cialdi, Stefano Olivares, Bassano Vacchini and Matteo G. A. Paris[†]

Quantum Technology Lab, Dipartimento di Fisica
Università degli Studi di Milano, I-20133 Milano, Italy

INFN, Sezione di Milano, I-20133 Milano, Italy
[†]matteo.paris@fisica.unimi.it

We unveil a novel source of non-Markovianity for the dynamics of quantum systems, which appears when the system does not explore the full set of dynamical trajectories in the interaction with its environment. We term this effect *non-Markovianity by undersampling* and demonstrate its appearance in the operation of an all-optical quantum simulator involving a polarization qubit interacting with a dephasing fluctuating environment.

Keyword: Quantum simulators.

1. Introduction

Non-Markovianity is a property of quantum dynamical maps which, loosely speaking, should capture the appearance of memory effects in the evolution of open quantum systems.[1–3] Such effects can be traced back to a backflow of information from the environment to the system, and their appearance is closely connected to a property of the dynamics known as divisibility.[4–11] Lack of this property reflects the fact that knowledge of the system state at a given time is not enough to determine its future evolution.

In those situations, where the open quantum system is coupled to a classical-like fluctuating environment,[12–15] the partial trace over the environment is usually obtained by averaging the dynamics over the realizations of the stochastic process that

describes its classical fluctuations. On the other hand, the possible non-Markovianity of the resulting dynamical map is not determined by the sole properties of the classical stochastic process. Rather, it results from an interplay between the structure of the interaction Hamiltonian, the time scale of the classical environment and the dimension of the open quantum system. In fact, a classical environment with fluctuations described by a (classically) non-Markovian process may induce either a Markovian or a non-Markovian quantum evolution, depending on the structure of the interaction Hamiltonian.[16,17]

Having these considerations in mind, in this paper we discuss and unveil a novel source of non-Markovianity for open quantum systems coupled to classical fields, which appears when the structure of the interaction does not allow the system to explore the full set of realizations of the stochastic process. In this case, the reduced dynamics of the open quantum system do not correspond to the averaging over the stochastic ensemble, since the system is not actually sensing all the possible trajectories of the environment. Rather, the average should be explicitly performed on the actual trajectories and the resulting dynamical map may be non-Markovian also when the ensemble-averaged one is Markovian.

We term this effect *non-Markovianity by undersampling* and demonstrate its appearance in optical platforms, that is, for polarization qubit interacting with a dephasing fluctuating environment. To this aim, we employ our recently developed all-optical quantum simulator.[18] In turn, our analysis may be considered as a benchmark to assess the performances of quantum simulators involving sampling of limited size.

It is worth noting that for open quantum systems subject to dephasing, an effective description in terms of the coupling with a classical fluctuating field is always viable.[19–21] The explicit construction of the corresponding classical stochastic process may indeed be obtained for a generic quantum environment.[21] Non-Markovianity by undersampling is thus expected to be a general feature, which is present in any system interacting with a structured environment inducing a dephasing dynamics. Besides, quantum environments may be described by classical fields, at least in the short-time limit, whenever global symmetries are available, leading to the definition of environmental operators that remain well defined when the size of the environment is increased.[22]

The paper is structured as follows: In Sec. 2 we introduce the model of the dynamics, in Sec. 3 we briefly describe the experimental setup and in Sec. 4 we present the experimental results and their analysis. Section 5 concludes with final remarks.

2. Model

Let us consider a single qubit interacting with a classical field via the (interaction) Hamiltonian $H_I = \lambda(t)\sigma_3$, where $\lambda(t)$ denotes a stochastic process describing the fluctuating field and σ_3 is a Pauli matrix. The corresponding evolution operator is

given by

$$U(t) = \exp\left\{-i \int_0^t H_I(s)ds\right\} = e^{-i\varphi(t)\sigma_3}, \tag{1}$$

where the time-dependent phase is given by $\varphi(t) = \int_0^t \lambda(s)ds$. If ϱ_0 denotes the initial state of the qubit, the state at time t is obtained by averaging over the realizations of the stochastic process, that is, the dynamical map corresponds to the ensemble average

$$\varrho(t) = \mathcal{E}(t)[\varrho_0] = \langle U(t)\varrho_0 U^\dagger(t)\rangle_\Lambda, \tag{2}$$

where the functional integral

$$\langle f[\lambda(t)]\rangle_\Lambda = \int \mathcal{D}[\lambda(t)]p[\lambda(t)]f[\lambda(t)] \tag{3}$$

is performed over all the possible trajectories of the stochastic process $\Lambda \equiv \lambda(t)$, $p[\lambda(t)]$ being its probability distribution and $\mathcal{D}[\lambda(t)]$ being the volume element of the probability space. On the other hand, if the interaction between the system and its environment is such that the number N of realizations is inherently small, then the dynamical map corresponds to the average over the actual realizations, i.e.

$$\varrho(t) = \mathcal{E}_N(t)[\varrho_0] = \frac{1}{N}\sum_k e^{-i\varphi_k(t)\sigma_3}\varrho_0 e^{i\varphi_k(t)\sigma_3}, \tag{4}$$

where $\varphi_k(t) = \int_0^t \lambda_k(s)ds$ denotes the phase-shift originating from the specific kth realization of the process. Of course, if the number of realizations is large, we are back to the ensemble average by the law of large numbers

$$\mathcal{E}_N(t)[\varrho] \overset{N\to\infty}{=} \mathcal{E}_\infty(t)[\varrho] \equiv \mathcal{E}(t)[\varrho]. \tag{5}$$

The properties of the dynamical maps $\mathcal{E}_N$ at finite N may be different from those of $\mathcal{E}$ and, in particular, $\mathcal{E}_N$ may be non-Markovian even if $\mathcal{E}$ is Markovian.

We perform simulations involving Gaussian noise and RTN, and we discuss the non-Markovianity of the dynamics. For Gaussian noise, we choose a paradigmatic example, the Ornstein–Uhlenbeck (OU) stochastic process,[23] which has been widely studied in the context of open quantum systems.[17,20,24] Both OU noise and RTN are characterized by an exponentially decaying correlation function, and hence by a Lorentzian spectrum. The statistics of the two stochastic processes, however, is completely different. For the RTN, each realization $\lambda_{\mathrm{RTN}}(t)$ jumps randomly between the two values $\pm\nu$, where ν is a coupling constant, with a switching rate γ. This means that, after a time t, the number of jumps that have occurred follows a Poisson distribution with parameter γt. Thus, in order to generate a sample of RTN noise, we discretize time with steps of length δt and at each step we perform a jump with probability $\delta P = 1 - e^{-\gamma\delta t}$. The initial state of the noise is chosen randomly between $+\nu$ and $-\nu$, with probability 50%.

For the OU process, on the other hand, we have $\lambda_{\mathrm{OU}}(t) = \nu B(t)$, where $B(t)$ satisfies the stochastic equation

$$B(t + \delta t) = (1 - 2\gamma\delta t)B(t) + 2\sqrt{\gamma}dW(t), \tag{6}$$

where $dW(t)$ is a Wiener increment with zero mean and variance, $\sigma^2 = \delta t$. For each realization we impose the initial condition $B(0) = 0$. For both models, an exact solution for Eq. (2) can be found.[25,26] It reads

$$\rho(t) = \frac{1}{2}[1 - G(t)]\sigma_3\rho_0\sigma_3 + \frac{1}{2}[1 + G(t)]\rho_0. \tag{7}$$

The function $G(t)$, known as the decoherence function, can be obtained analytically for both noises. For RTN it reads

$$G_{\mathrm{RTN}} = e^{-\gamma t}(\cosh\eta t + \eta^{-1}\gamma\sinh\eta t), \tag{8}$$

where $\eta = \sqrt{\gamma^2 - 4\nu^2}$. For the OU noise

$$G_{\mathrm{OU}} = e^{-2\nu^2\beta(t)}, \quad \beta(t) = \frac{1}{2\gamma^2}(e^{-2\gamma t} + 2\gamma t - 1). \tag{9}$$

To work with adimensional units, in the following we redefine t as νt and γ as γ/ν.

Among the different criteria that have been devised to characterize the non-Markovianity of a quantum map, we employ the one introduced by Breuer *et al.*,[27] which links the presence of a backflow of information from the environment to the system to a temporary increase of the distinguishability among different initial states of the system evolved according to the same reduced dynamics. The distinguishability between states is quantified by their trace distance, defined as

$$D(t) = \frac{1}{2}\|\rho_1(t) - \rho_2(t)\|_1, \tag{10}$$

where we denote $\|A\|_1 = \mathrm{Tr}\sqrt{A^\dagger A}$ as the trace norm of the operator A. A map is non-Markovian if there exists a pair of initial states $\rho_1(0), \rho_2(0)$ for which $D(t)$ is not monotonically decreasing in time.

In Ref. 27, a measure $\mathcal{N}$ is introduced in order to quantify the degree of non-Markovianity. It is defined as the time integral of the derivative of the trace distance on the time intervals where it is increasing, that is

$$\mathcal{N}(\mathcal{E}) = \frac{1}{2}\max_{(\rho_1,\rho_2)}\int_0^\infty(\dot{D}_{12}(t) + |\dot{D}_{12}(t)|)dt, \tag{11}$$

where

$$\dot{D}_{12}(t) = \frac{d}{dt}D(\rho_1(t), \rho_2(t)), \tag{12}$$

and the maximization is over all possible pairs of initial states of the dynamics. $\mathcal{N}(\mathcal{E})$ is clearly zero if the map $\mathcal{E}$ is Markovian, and it is greater the more the trace distance deviates for a monotonically decreasing behavior.

For single-qubit dephasing channels as in Eq. (7), the optimal pair of states to witness non-Markovianity is known to be the pair $|\pm\rangle = (|H\rangle \pm |V\rangle)/\sqrt{2}$.[3] The trace distance between these two states is $D(\rho_+(t), \rho_-(t)) = |G(t)|$, where $\rho_\pm = |\pm\rangle\langle\pm|$. Thus, a non-monotonic behavior of the decoherence function $G(t)$ is a necessary and sufficient condition for the non-Markovianity of the channel. Starting from the above formula for $D(\rho_+(t), \rho_-(t))$, it is clear that the dephasing map induced by the Gaussian stochastic process is Markovian, as $\beta(t)$ is a monotonically increasing function of t, while RTN gives a non-Markovian map for $\gamma < 2$.[25] But if the dynamics of the qubit is given by a finite number of realizations of the stochastic process, Eq. (4), then the above conclusions are no longer valid.

3. Experimental Apparatus

In order to demonstrate the non-Markovianity by undersampling, we exploit our recently developed quantum simulator.[18] This simulator can perform the evaluation of Eq. (4) using the polarization of a single photon as a qubit and exploiting its spectral components to average over the realizations of the stochastic dynamics. In particular, we consider the qubit affected by dephasing driven either by Gaussian noise or non-Gaussian random-telegraph noise (RTN). These are interesting examples since, in both cases, the ensemble average of Eq. (2) may be performed analytically and it is known that Gaussian noise is leading to a Markovian map, whereas
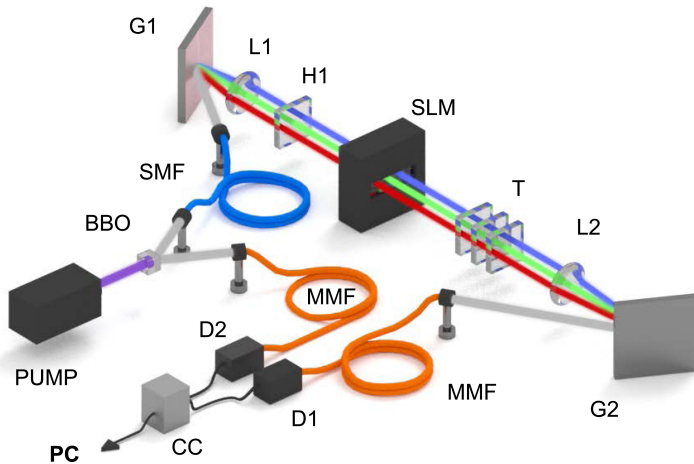

Fig. 1. Schematic diagram of our setup. The pump is a 405.5 nm laser diode; a couple of frequency-entangled photons is generated via parametric down-conversion (PDC) through a BBO, Beta barium borate nonlinear crystal; one photon is sent via a multi-mode fiber (MMF) to the single-photon detector D2. The other is sent through a single-spatial-mode and polarization preserving fiber (SMF) to the 4F system. The 4F system is composed of two diffraction gratings G1-G2, two lenses L1-L2, a half-wave plate H1 that prepares the photon in the initial state $|+\rangle$, the spatial light modulator (SLM), and a tomographic apparatus T, made of a quarter-wave plate, a half-wave plate and a polarizer. The photon is then sent through a MMF to the single-photon detector D1. Finally, an electronic device measures the coincidence counts (CC) and sends them to the computer (PC).

RTN noise may originate both Markovian and non-Markovian maps depending on the values of its switching rate.[25]

Our experimental setup is sketched in Fig. 1 and described in detail in Ref. 18. Frequency-entangled photon pairs are generated by parametric down-conversion (PDC) and then collected by two fiber couplers. The idler photon is detected after traveling through a multimode fiber (MMF). The signal photon enters a 4F system and is then coupled to a MMF and reaches the single photon detector. Coincidence counts with the idler photon are then detected. The key ingredient of the simulator is a spatial light modulator (SLM), placed on the Fourier plane between the two lenses L1 and L2 of the 4F system. The SLM is a 1D liquid crystal mask (640 pixels) used to introduce a different phase (externally controlled by the PC) to each pixel. The PDC spectrum, selected with a rectangular profile through a slit, hits 64 pixels. A phase $\varphi_k(t)$ is assigned to each group of pixels, implementing the simulation of the dynamical map in Eq. (4). The average over the realizations of the noise is thus performed by (coherently) collecting the different spatial components through the lens L2 and the grating G2 into a MMF. The state reconstruction is performed by the tomographic apparatus T placed between the SLM and the L2 lens.

4. Results

With the apparatus described above, we simulated the interaction of the qubit, initially prepared in the state $|+\rangle$, with RTN and OU noise, with $\gamma = 4$. For $\gamma = 4$, the RTN is in the fast regime and thus for both kinds of noise the dynamics is Markovian when considering the ensemble average, Eq. (2). To perform the simulation, we discretize the time interval $\{0, t_1, \ldots, t_n\}$ (with step $\Delta t = 0.001$) and generate on a computer the required number of realizations of each type of noise $\lambda_k(t_i)$. Then for each output time step t_i, the accumulated phases $\varphi_k(t_i) = \int_0^{t_i} \lambda_k(t)dt$ are encoded in blocks of adjacent pixels in order to use the maximum number of available pixels. A photon initially prepared in the $|+\rangle$ state is sent through the SLM and its state is then reconstructed via a tomography, with four projective measurements.[28–31] The acquisition time is 10 s.

From the off-diagonal element of the density matrix we can obtain the decoherence function $G(t)$ and hence the optimal trace distance. The appropriate corrections are implemented to take into account imperfections in the experimental apparatus. The initial state of the photon is not exactly ρ_+, but rather a combination with the maximally mixed state:

$$\rho_{0,\exp} = p\rho_+ + (1 - p)\mathbb{I}/2, \tag{13}$$

where $\mathbb{I}$ is the identity operator and $p \sim 0.98$.

The results are summarized in Fig. 2, which shows the evolution of the trace distance as a function of time for the two noises, comparing experimental data (points) with a simulation (solid, shaded lines) and with the analytical solution of the

ensemble-averaged map, Eq. (2). From top to bottom, the number of realizations of the noise that are simulated in the SLM increases. We clearly see that the trace distance has revivals, thus witnessing the non-Markovianity of the quantum evolution. The behavior of the map is similar between the two kinds of noise. The lower the number of realizations, the more pronounced are the revivals. For 64 realizations of the noise, the evolution of the trace distance is close to the ensemble-averaged map.

We now seek to find a relation between the non-Markovianity of the quantum map of Eq. (4) and the number N of trajectories that build up the map. A quantitative analysis must rely on a measure of the degree of non-Markovianity of the dynamics. We employ the one introduced in Eq. (11), based on the backflow of information from the environment to the system, using the pair of optimal initial states $(|+\rangle, |-\rangle)$. The results are presented in Fig. 3. The map $\mathcal{E}_N(t)$ depends on the actual realizations of the noise and thus we consider the average $\overline{\mathcal{N}}$ of the non-Markovianity measure $\mathcal{N}$ over a large number of repetitions of the experiment. In the left panel, $\overline{\mathcal{N}}$ is presented as a function of the number of realizations N of the noise, for both OU and RTN. We can see that it decreases monotonically with N, although the functional dependence is not trivial. On the right panel, the probability density function of $\mathcal{N}$ for different simulation is presented for three different values of N, showing that, with increasing N, the distribution gets more peaked around the average $\overline{\mathcal{N}}$.

From the above considerations a question arises on whether we may link the non-Markovianity of the map $\mathcal{E}_N$ to its *distance* from the asymptotic one $\mathcal{E}_\infty$. As we will see, this is indeed the case. As a measure of the distinguishability, we employ the *infidelity*

$$\Delta_N \equiv \Delta_N(\mathcal{E}_N, \mathcal{E}_\infty) = 1 - \mathcal{F}(\mathcal{E}_N, \mathcal{E}_\infty), \tag{14}$$

where the fidelity $\mathcal{F}(\mathcal{E}_N, \mathcal{E}_\infty)$ between channels is defined as the state fidelity between the Choi–Jamiołkowski (CJ) states of the two channels.[32] Given the maximally entangled state between the qubit and an ancilla, $|\Psi\rangle = (|00\rangle + |11\rangle)/\sqrt{2}$, the CJ state of a map $\mathcal{E}$ is $\rho_\mathcal{E} = (\mathbb{I} \otimes \mathcal{E})(|\Psi\rangle\langle\Psi|)$. After a straightforward calculation, we then obtain the infidelity between the channels $\mathcal{E}_\infty(t)$ and $\mathcal{E}_N(t)$ (for the sake of simplicity we drop the explicit dependence on t of G and G_N):

$$\Delta_N(t) = \frac{1}{2}[1 - G\mathrm{Re}[G_N] - \sqrt{(G^2 - 1)(|G_N|^2 - 1)}], \tag{15}$$

where $G_N = \langle e^{-2i\varphi_k}\rangle_N$. Note that in the limit $N \to \infty$ we have $G_N \to G$ and, thus, $\Delta_N(t) \to 0$.

The map $\mathcal{E}_N(t)$ depends on the actual realizations of the noise and thus we consider the average $\overline{\mathcal{F}_\mathcal{N}}(t)$ of the fidelity over a large number of repetitions of the experiment. The left panel of Fig. 4 shows the infidelity Δ_N for particular realizations of the experiment with a low number of trajectories of the noise, while the right panel shows the same quantity averaged over a high number of repetitions. From the latter,
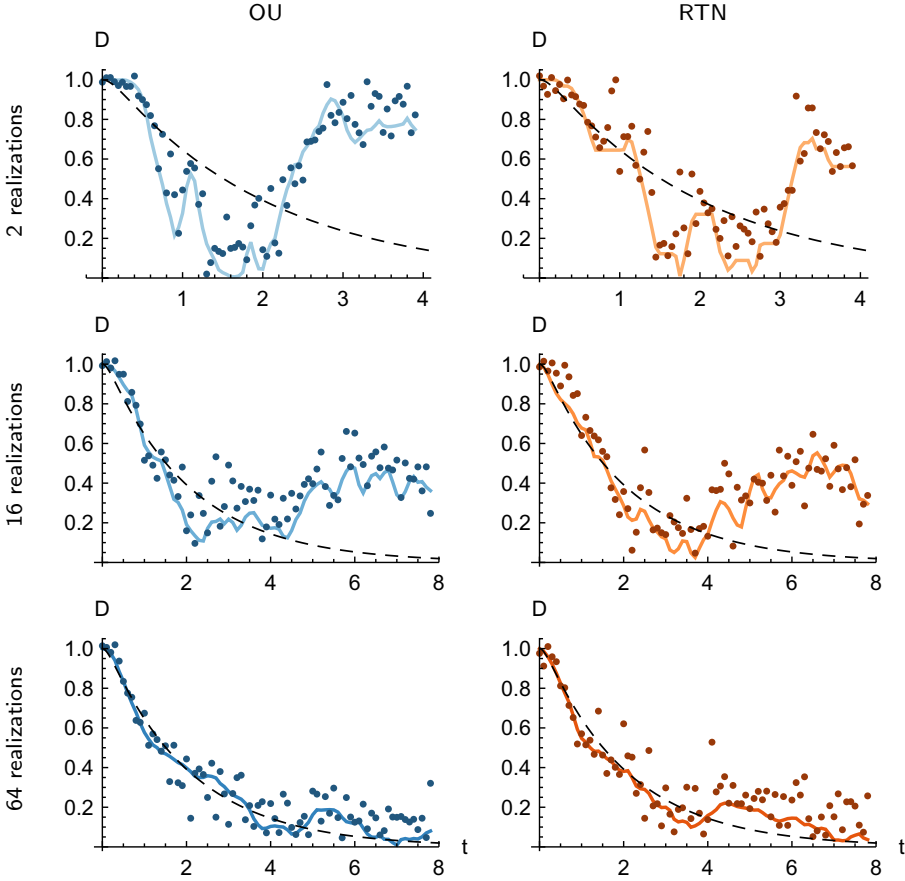
Fig. 2. Evolution of the trace distance with time for the OU noise (left) and RTN (right) for 2, 16 and 64 realizations of the noise (from top to bottom), with $\gamma = 4$. The points represent experimental data, while the solid curve is the simulated trajectory. For comparison, the dynamics resulting from the ensemble-averaged noise is shown with the black dashed line. The trace distance has revivals that are more pronounced for lower numbers of realizations. This is a clear signature of the non-Markovianity of the map, in contrast with the analytical solution of Eq. (7) that shows a monotonic behavior.

we can see that the average infidelity $\overline{\Delta_N}$, starting from zero, reaches a value that is constant in time and depends on the number of trajectories of the noise.

We have then investigated the dependence of this value on N and its connection with the non-Markovianity. The results are presented in Fig. 5, where the average over time of $\overline{\Delta_N}$ is shown as a function of N, for the OU noise and RTN, averaged over time. The infidelity decreases with N as does the non-Markovianity (cf. Fig. 3). The right panel clearly shows that there is a monotonic dependence of the non-Markovianity measure on the average infidelity between the undersampled channel and the ensemble-averaged one.
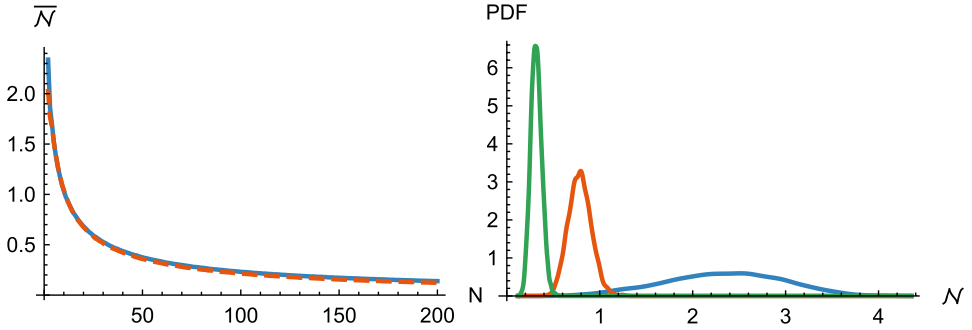
Fig. 3.   (Color online) Left panel: Average non-Markovianity $\overline{\mathcal{N}}$ on the time interval $t \in [0, 8]$, obtained by repeating the simulation 5,000 times, as a function of the number of realizations N of the noise. The solid blue line is for the OU noise, the dashed orange line is for the RTN. Right panel: the distribution of the values of $\mathcal{N}$ for the OU noise, for the number of realizations of Fig. 2: $N = 2$ (blue), $N = 16$ (orange), $N = 64$ (green).
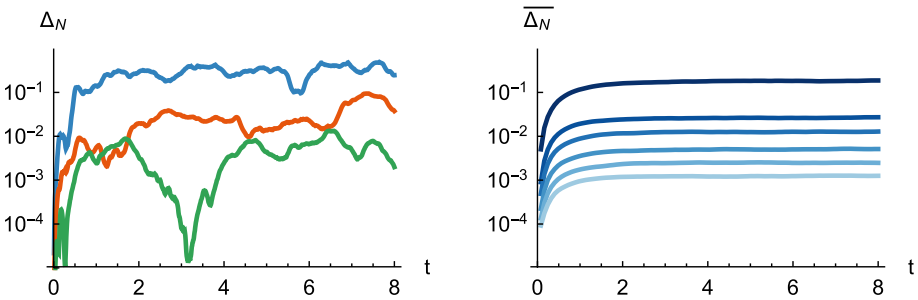

Fig. 4.   (Color online) In the left panel, infidelity Δ_N as a function of time for $N = 2$ (blue), $N = 16$ (orange), $N = 64$ (green) for OU noise. In the right panel the same quantity, averaged over 5,000 repetitions of the experiment, for (top to bottom) 2, 10, 20, 50, 100 and 200 trajectories of the noise. We can see that the average fidelity saturates to a constant value that depends on N.
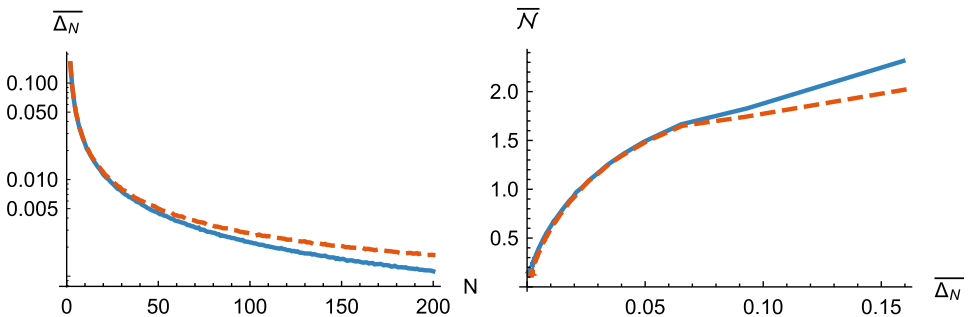

Fig. 5.   (Color online) Left panel: Log–log plot of the average over 5,000 repetitions of the time averaged infidelity $\overline{\Delta_N}$, as a function of the realizations of the noise for the OU (solid blue) and RTN (dashed orange). As the number of trajectories increases, the infidelity vanishes, as does the BLP measure of non-Markovianity. Right panel: Average BLP measure of non-Markovianity $\overline{\mathcal{N}}$ as a function of the average infidelity $\overline{\Delta_N}$. Note the monotonic, although nontrivial relation between the two quantities.

5. Conclusions

In this paper, we have introduced, demonstrated and discussed *non-Markovianity by undersampling*, a phenomenon which appears in the dynamics of quantum systems interacting with structured environments, when the system does not explore the full set of dynamical trajectories. We have demonstrated experimentally its appearance using an all-optical quantum simulator built with a polarization qubit interacting with a dephasing fluctuating environment. Our results clearly indicate that non-Markovianity is quantitatively linked to the *infidelity* between the undersampled channel and the ensemble-averaged asymptotic one.

Our results pave the way for a deeper understanding of the origin of non-Markovianity in dephasing quantum channels and represent a benchmark to assess the performances of quantum simulators involving sampling of limited size.

Acknowledgments

References

1. H.-P. Breuer, *J. Phys. B* **45** (2012) 154001.
2. A. Rivas, S. F. Huelga and M. B. Plenio, *Rep. Prog. Phys.* **77** (2014) 094001.
3. H.-P. Breuer, E.-M. Laine, J. Piilo and B. Vacchini, *Rev. Mod. Phys.* **88** (2016) 021002.
4. M. M. Wolf, J. Eisert, T. S. Cubitt and J. I. Cirac, *Phys. Rev. Lett.* **101** (2008) 150402.
5. A. Rivas, S. F. Huelga and M. B. Plenio, *Phys. Rev. Lett.* **105** (2010) 050403.
6. D. Chruściński, A. Kossakowski and A. Rivas, *Phys. Rev. A* **83** (2011) 052128.
7. S. Wißmann, H.-P. Breuer and B. Vacchini, *Phys. Rev. A* **92** (2015) 042108.
8. X.-M. Lu, X. Wang and C. P. Sun, *Phys. Rev. A* **82** (2010) 042103.
9. F. Benatti, R. Floreanini and S. Olivares, *Phys. Lett. A* **376** (2012) 2951.
10. F. F. Fanchini, G. Karpat, B. Çakmak, L. K. Castelano, G. H. Aguilar, O. J. Farías, S. P. Walborn, P. H. S. Ribeiro and M. C. de Oliveira, *Phys. Rev. Lett.* **112** (2014) 210402.
11. S. Haseli, G. Karpat, S. Salimi, A. S. Khorashad, F. F. Fanchini, B. Çakmak, G. H. Aguilar, S. P. Walborn and P. H. S. Ribeiro, *Phys. Rev. A* **90** (2014) 052118.
12. D. Zhou, A. Lang and R. Joynt, *Quantum Inf. Process.* **9** (2010) 727.
13. A. D'Arrigo, R. L. Franco, G. Benenti, E. Paladino and G. Falci, *Phys. Scr.* **2013** (2013) 014014.
14. E. Paladino, Y. M. Galperin, G. Falci and B. L. Altshuler, *Rev. Mod. Phys.* **86** (2014) 361.
15. C. Benedetti, F. Buscemi, P. Bordone and M. G. A. Paris, *Phys. Rev. A* **87** (2013) 052328.
16. C. Addis, B. Bylicka, D. Chruściński and S. Maniscalco, *Phys. Rev. A* **90** (2014) 052103.
17. M. A. C. Rossi and M. G. A. Paris, *J. Chem. Phys.* **144** (2016) 024113.
18. S. Cialdi, M. A. C. Rossi, C. Benedetti, B. Vacchini, D. Tamascelli, S. Olivares and M. G. A. Paris, *Appl. Phys. Lett.* **110** (2017) 081107.
19. D. Crow and R. Joynt, *Phys. Rev. A* **89** (2014) 042123.
20. C. Benedetti and M. G. A. Paris, *Int. J. Quantum Inf.* **12** (2014) 6.
21. A. Chenu, M. Beau, J. Cao and A. del Campo, *Phys. Rev. Lett.* **118** (2017) 140403.

22. M. A. C. Rossi, C. Foti, A. Cuccoli, J. Trapani, P. Verrucchi and M. G. A. Paris, *Phys. Rev. A* **96** (2017) 032116.
23. G. E. Uhlenbeck and L. S. Ornstein, *Phys. Rev.* **36** (1930) 823.
24. T. Yu and J. H. Eberly, *Opt. Commun.* **283** (2010) 676.
25. C. Benedetti, M. G. A. Paris and S. Maniscalco, *Phys. Rev. A* **89** (2014) 012114.
26. M. A. C. Rossi, C. Benedetti and M. G. A. Paris, *Int. J. Quantum Inf.* **12** (2014) 1560003.
27. H.-P. Breuer, E.-M. Laine and J. Piilo, *Phys. Rev. Lett.* **103** (2009) 210401.
28. K. Banaszek, G. M. D'Ariano, M. G. A. Paris and M. F. Sacchi, *Phys. Rev. A* **61** (1999) 010304.
29. D. F. V. James, P. G. Kwiat, W. J. Munro and A. G. White, *Phys. Rev. A* **64** (2001) 052312.
30. S. Cialdi, F. Castelli, I. Boscolo and M. G. Paris, *Appl. Opt.* **47** (2008) 1832.
31. S. Cialdi, A. Smirne, M. G. A. Paris, S. Olivares and B. Vacchini, *Phys. Rev. A* **90** (2014) 050301(R).
32. M. Raginsky, *Phys. Lett. A* **290** (2001) 11.